Inference of Neutral Particle Trajectories in a Hydrogen Bubble Chamber using Digital Techniques for Increased Accuracy

Joshua G. Albert
University of Toronto

Abstract

A computer program named Bubbles to Momentum (BuM) was written to make accurate momentum measurements on two slides from a previous bubble chamber experiment carried out at the Stanford Linear Accelerator Centre. BuM's level of accuracy positively validated conservation of energy. A calibration of the slide projection table found 1mm on the projection table was equal to 1.113 ± 0.0062mm in the bubble chamber. The use of an energy-distance relation was found helpful in identifying some tracks though it suffered from a low resolution of accuracy.

1 Introduction

High energy physics has a long history of progress since the days of Albert Einstein. In this experiment two films taken at the Stanford Linear Accelerator Centre (SLAC), with particle trajectories within 10° of being two dimensional, were analyzed. A set of events on each film were studied after first coding a computer program for the task to reduce measurement error. The conservation of momentum was used to verify the existence of neutral particles, and conservation of energy, strangeness and charge, with the help of an energy-distance relation, are used to specify the particle. An effort is made to reduce uncertainty.

2 Theory

In this theory we use tensor notation, and Einstein summation notation to express our equations. A rank-one tensor is given by, v^a, a rank-two tensor by, J^{ab}, etc. The inner product in four dimensions for a four-vector, $v^a = (v^t, v^x, v^y, v^z)$, is defined in Einstein summation notation as a contraction of a pair of one upper and one lower index,

$$\begin{aligned} ||v|| &= v^a v_a \\ &= v_t^2 - (v_x^2 + v_y^2 + v_z^2). \end{aligned} \tag{1}$$

2.1 Conservation of Invariant Mass

In high energy physics we must take into account the special relativistic effects of Lorenz boosts. Each particle is given an invariant mass, m, and four-momentum, $p^a = (E/c, p)$. We will set $c = 1$ here and measure all our quantities in appropriate units. Thus our four momentum is,

$$p^a(E, p) \tag{2}$$

and it satisfies the relation,

$$p^a p_a = E^2 - p^2 = m^2. \tag{3}$$

Here energy takes into account the kinetic as well as rest mass,

$$E = \gamma m c^2 \quad \text{showing } c \text{ for clarity,} \tag{4}$$

where,

$$\gamma = \frac{1}{\sqrt{1 - \frac{v^2}{c^2}}}, \tag{5}$$

thus we can see that if we measure energy in MeV we can measure mass in units of MeV/c^2, and momentum in units of MeV/c. Energy and momentum are not conserved in arbitrary frames. Moreover, they are only conserved in the same reference frame. Invariant mass, equation 3, is invariant in all frames.

2.2 Decays

In decays we will be most concerned with neutral particles decaying to two charged particles. In this case measurement of the outgoing momentums of the charged particles yields the incoming particles' momentum. Using conservation of charge there should be a negative and positive particle in evidence.

Consider a particle with energy, E, in the lab frame decaying into many, $A \rightarrow C_1 + ... + C_n$. Initially we have $p^a = (E, p)$. After the decay in the same lab frame we have, $p_i^a = (E_i, p_i)$. We must have conservation of energy, so using equation 3,

$$\sqrt{m_a^2 + p^2} = \sum_i^N \sqrt{m_i^2 + p_i^2}, \tag{6}$$

where we must keep the same lab frame for this to hold. Supposing we knew the masses of particles $C_1, ..., C_N$ we could then calculate m_a for the incoming neutral particle.

2.3 Scattering

In scattering we consider two particles colliding and producing extra particles, $A + B \rightarrow C_1 + ... + C_n$. We take B to be a rest in the lab frame, and A to have energy E, thus before the collision, $p^a = (E + m_b, p_a)$, implies,

$p^a p_a = 2E m_b + m_b^2 + m_a^2$.

After the collision we have, in the CM frame, $p'^a = (M \equiv \sum_i^n m_i, 0)$, which implies by invariance of equation 3,

$$E = \frac{M^2 - m_a^2 - m_b^2}{2m_b}. \quad (7)$$

We can use equation 7 as a condition for helping determine the invariant masses of the particles produced in scattering. Suppose a neutral particle is produced in a scattering which then decays later into two particles. We could then use equation 6 to relate the decay products to the scattering event by substitution into equation 7.

In our experiment positive pions often hit a proton, nearly at rest, to produce many pions. Assuming that only charged pions are produced then there must be an even number of them. We find that our pion beam could produce at most 12 pairs of pions using equation 7.

2.4 Conservation of Strangeness

The timescales of the three interactions are 10^{-23}s for the strong, 10^{-16}s for the electromagnetic, and 10^{-13}s for the weak interactions. In general the process will be governed by the fastest interaction which is kinematically allowed.

The standard model tells us that strangeness, the number of strange quarks in a system, must be conserved for strong and electromagnetic interactions. It need not be conserved in weak interactions but its value may only change by one unit per interaction. Total baryon number must always be conserved.

A pion colliding with a proton has a kinematically allowed strong interaction. It is particle production via scattering, the same one mentioned in section 2.3. Initially, there is a 0S (strangeness), hence the produced particles must have total 0S. Often a kaon meson, K^0, or lambda baryon, Λ^0, will be produced. The quark content of these are $d\bar{s}$, and uds, with strangenesses -1S and 1S, respectively. Though other neutral strange particles are possible only these are considered in this experiment.

2.5 Radius of Curvature of Trajectories

Within our bubble chamber there is magnetic field pointing out of the slide. From our standard electromagnetism theory we know that a charged particle will follow a curved trajectory in a magnetic field, the direction of curve given by the Lorentz force. The parameters of the SLAC bubble chamber are such that a charged particle moving in a circular trajectory of radius R will have a magnitude of momentum given by,

$$|p| = \frac{R}{1890\text{mm}}\text{GeV/c}, \quad \text{where R is in mm.} \quad (8)$$

The problem on uncertainty thus relies on how accurately one can measure the radius of a track. Using a straight edge, compass, and geometry one can construct the exact solution of a circle passing through any three non-collinear points, say $\{P,Q,R\} = \{(x_1,y_1),(x_2,y_2),(x_3,y_3)\}$. The method proceeds as: draw two lines between the points, say PQ and QR. Construct the perpendicular bisector of each line with your compass. Where the perpendicular bisectors intersect is the centre of the circle. Connect your compass to the centre and any of three points and draw a circle. Mathematically we can do this. We find the centre, (x_c, y_c), and radius, R,

$$m_1 = \frac{y_2 - y_1}{x_2 - x_1}, \quad m_2 = \frac{y_3 - y_2}{x_3 - x_2},$$
$$x_c = \frac{m_1 m_2 (y_1 - y_3) + m_2(x_1 + x_2) - m_1(x_2 + x_3)}{2(m_2 - m_1)}, \quad (9)$$
$$y_c = \frac{x_1 + x_2}{2m_1} - \frac{x_c}{m_1} + \frac{y_1 + y_2}{2}, \quad (10)$$
$$R = \sqrt{(y_1 - y_c)^2 + (x_1 - x_c)^2}. \quad (11)$$

Equations 9–11 are easily calculable by a computer.

2.6 Energy-Distance Relation

Knowing a particle's momentum does not identify the type of particle in most cases. Early work done on charged particle trajectories in bubble chambers [2] discuss a range-energy relation where the characteristics of a track can help identify the particle. Figure 1 shows this relation. For fast particles the track will be

thinner with more distance between bubbles [4]. Interpolating momentum on figure 1 can, in some cases, tell an experimenter which particle the track is. Measurement of the track characteristics methodically is important in this process. The computer can again help by making more precise measurements of track thicknesses.

Slower particles ionize the hydrogen more, thus we define the incoming pion beam as minimum ionizing and compare all tracks to it. The way to use figure 1 is to interpolate our our momentum onto $\frac{dE}{dx}$, which are the dashed lines, then divide this value by the asymptotic value of 0.24MeV cm^{-1} to get the relative ionization value. Note that there are four dashed lines; one for each the muon, pion, kaon, and proton. A high relative ionization should show a darker, thicker track, while minimum ionizing will look like one of the incoming pion tracks.

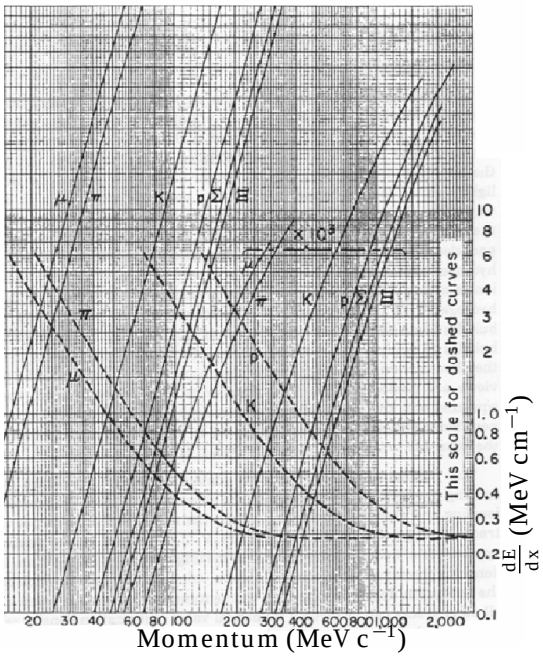

Figure 1: Energy-distance relation as a function of momentum. The right hand scale is used for the dashed lines to calculate the relative ionizations of a track for the different possibilities of muon, pion, kaon, and proton. The identification then depends on whether the track fits the characteristics one of the values.

3 The Experiment

For the experiment a program was written, named Bubbles to Momentum (BuM), that enabled a user to look at scanned copies of the film taken a SLAC experiment, shown schematically in figures 2 and 3. It uses the technique from section 2.5 to measure the radii of tracks. The program was written in MATLAB©in order to take advantage of the simple visualization and interface libraries. The program is able to work with two tracks at a time and compute from them the total momentum of a decaying particle, or the momentum of an invisible particles, using options 'X $\rightarrow 1+2$' or '$1 \rightarrow X+2$', respectively. Pressing 'h' while the program window is in focus brings up an information screen on how to use the program most effectively. The program also allows measurement on angles between tracks, width of tracks, and interpolation of momentum of relative ionicity using data taken from figure 1.

The pion beam has an energy of 10.3GeV. The slides are projected on a table. Using the pion energy and the information from section 2.5 a calibration was done on the scaling, and it was found 1 mm on the table is equivalent to 1.113 ± 0.0062mm in the bubble chamber.

After using the program to measure the momentums, widths, and possible relative ionizations of all tracks shown in figures 2 and 3, conservation of energy, equations 7 and 6, and conservation of strangeness were used to infer to types of particles for both the visible and invisible tracks.

4 Results

The momentums of tracks, in figures 2 and 3, are tabulated in table 1, and the possible relative ionizations in table 2. The uncertainties are discussed in section 5.3 below.

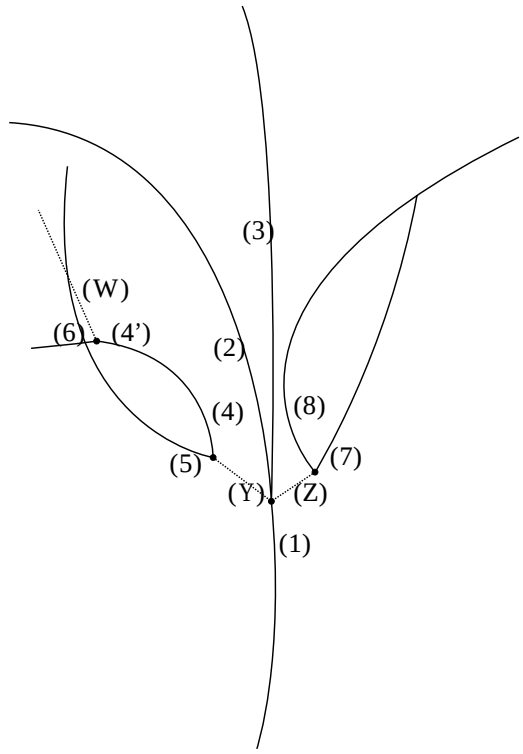

Figure 2: View 1, film 164, slide 872 from a SLAC experiment. The dashed lines are invisible particles inferred from conservation of momentum in the experiment. The incoming pion enters from the bottom and is track (1).

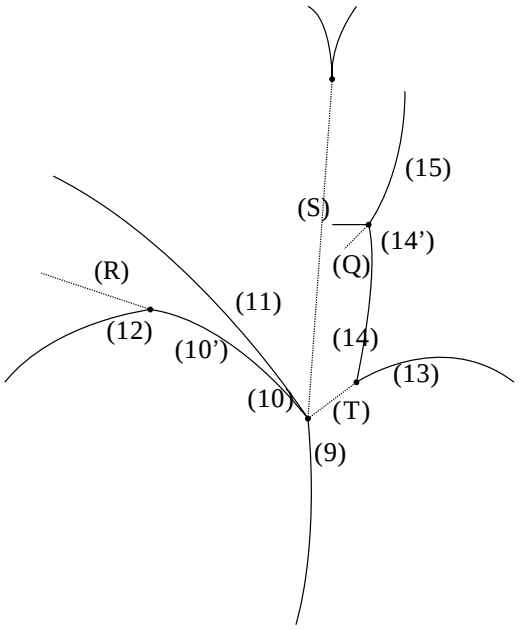

Figure 3: View 2, film 254, slide 810 taken from a SLAC experiment. The dashed lines are invisible particles inferred from conservation of momentum in the experiment. The incoming pion enters from the bottom and is track (9). Track (Q) encompasses two visible and invisible tracks.

5 Discussion

5.1 Slide 872

From table 2 it is possible to identify some tracks' particles. Looking at tracks (1) and (9) it is clear that minimum ionizing pion tracks have a width near 1.14 ± 0.40mm. Tracks (Y) and (Z) undergo weak decays, judging by the wide 'V' angle characteristic of such decays [4]. The decay distance, τc, of K^0 is 2.68cm (we mean K_S^0, since the K_L^0 decay distance is on the order of 15m), and the Λ^0 decay distance is 7.89cm. This lends evidence toward (Z) and (Y) being K^0 and Λ^0 respectively. Track (2) appears to be a proton if line thickness correlates at all with relative ionization, however using energy conservation a better fit would be track (2) is a π^+ and (3) a p. We find in this configuration, $E_2 + E_3 + E_Y + E_Z = 10.836 \pm 0.2296$GeV, and given that the incoming pion beam, 10.3GeV, has some uncertainty, this configuration seems most plausible. This implies line thickness does not correlate well with relative ionization, probably due in part to the large uncertainty in line thickness.

Table 2 would imply tracks (4) and (5) are either kaons or protons with the chance that (4) could also be a pion since uncertainty in line width is large. Looking at the most frequent modes of decay of the Λ^0 shows a 62% decay ratio for $\Lambda \rightarrow p\pi^-$, however the proton could not decay to tracks (6) and (W). By the principle of detailed balance it is most probable that (4) is a π^+ and (5) is $\bar{p}$, which is in reasonable agreement with table 2. Thus, since track (6) must decay from a pion, it should be a μ^+ and (W) a ν_μ. Checking energy conservation, $E_4 + E_5 = 1.341 \pm 0.0070$GeV which is in good agreement with $E_Y = 1.326 \pm 0.0068$GeV, and $E_6 + E_W = 0.296 \pm 0.0369$GeV which is also in good agreement with $E_{4'} = 0.278 \pm 0.0081$GeV.

Likewise, K_S^0 has a decay ratio of 69% for $K_S^0 \rightarrow$

$\pi^+\pi^-$. Table 2 places this within the bounds of uncertainty. Checking energy conservation $E_7 + E_8 = 0.677 \pm 0.0105\text{GeV}$ which is in good agreement with $E_Z = 0.774 \pm 0.0088\text{GeV}$.

5.2 Slide 810

Track (S) is a neutral particle whose inferred existence stems from conservation of momentum. It could be two neutral particles, but operating under the assumption that it is just one particle, its track passes directly through the opening of a narrow 'V' in the upper part of the slide, as shown in figure 3. The narrowness of this angle implies [4] it may in fact be pair production, $\pi^0 \rightarrow e^+e^-\gamma$. Measurement of the momentums of the two tracks in the decay of (S) show there is missing momentum, which would be carried by the photon, γ. Hence track (S) adds no strangeness or charge and is possible if kinematically allowed by energy conservation.

Since (S) adds no strangeness, and assuming track (T) carries some strangeness then either (track (10) or (11) must be a K^+ with $-1S$, implying (T) must be have $+1S$ and hence is a Λ^0.

Table 2 implies that track (13) is either a μ^- or π^-. Assuming track (T)is a Λ^0, which has a decay fraction involving the μ of $1.57 \cdot 10^{-4}$, it is highly improbable for (13) to be a muon. Thus, taking (13) to be a π^-, (14) should be a p. Checking energy conservation, $E_{13} + E_{14} = 1.365 \pm 0.0382\text{GeV}$ which is in very good agreement with $E_T = 1.374 \pm 0.0346\text{GeV}$.

Table 2 is not very helpful in determining tracks (10) and (11), but note that taking (10) as a π^+, and (11) as a K^+ is plausible in the bounds of uncertainty. Under this configuration energy conservation is well within the bounds of uncertainty, $E_{10}+E_{11}+E_S+E_T = 11.238 \pm 0.968\text{GeV}$ while $E_9 = 10.332 \pm 0.1790\text{GeV}$. Furthermore, supposing track (10) decays into a μ^+ and ν_μ again energy conservation is nicely conserved, $E_{12} + E_R = 0.296 \pm 0.0310\text{GeV}$ matches nicely with $E_{10'} = 0.300 \pm 0.0252\text{GeV}$.

Comparing tracks (1), and (9) with (15) in table 2 implies that (15) is likely a π^+. The problem comes from looking at track (Q) that there are two tracks, as shown in figure 3. The dashed line does not match with the visible track implying that it may indeed be two particles. A π^- and π^0 seem most likely and indeed looking at energy conservation, $E_{15} + E_Q(\pi^0 + \pi^-) = 1.211 \pm 0.0566\text{GeV}$ matches nicely with $E_{14'} = 1.215 \pm 0.0494\text{GeV}$.

5.3 Error in Computer Calculations

Equations 9–11 rely upon two things. Calibration error from converting pixels (px) to mm, and how closely we can choose points in the centre of a line since they are several px wide.

The conversion of px to mm has the form, $L = L' \frac{s_{mm}}{s_{px}}$, where L is the length in the bubble chamber, L' is the length in px on the digitalized film, s_{mm} is a calibration scale in mm, and s_{px} is the corresponding calibration in px. These have measurement errors of $\Delta L'$, Δs_{mm}, and Δs_{px}. As a source of calibration the rakes on the film were used, which are evenly separated markings along the length of the bubble chamber. Hence Δs_{mm}, and Δs_{px} correspond to how accurately the rakes can be measured on the table and digitally. Those uncertainties are minimized by using Vernier callipers and zooming in on pixels. Also we must take into account the possibility that the racks may not be uniformly separated and that the film may have been skewed during the scanning process to digitize it. We account for these last two with a small percentage uncertainty of 0.5% since the rakes appear to be relatively uniformly separated but there is a slight skew apparent.

$\Delta L'$ is due to the fact that the track is several pixels wide and it is difficult to correctly select the centre of it for the circle parameter calculation. At first, centre of moment calculations were used to locate the centre of the track. This was implemented, by taking the average position of pixels weighted by the intensity of the pixels for a small neighbourhood about the track [3]. It yielded incorrect results since the tracks are formed of non-uniform bubbles. For our estimate of error it was found the best we can do is zoom in on a track and take the median pixel in a track cross-section, thus we suppose an initial measurement error of $1/e$ of a pixel.

The uncertainty still suffers from choice of a selection of points by a human user. In particular, tracks that are nearly straight will have a high uncertainty, as the perpendicular bisectors approach being parallel. To reduce this an average of multiple circle parameters are taken by selecting many points along a track. This reduces the uncertainty by a factor of $\sqrt{N}$ for N averages.

We thus use propagation of error on equations 9–11 and take the average to calculate uncertainty, using $\Delta L'$, Δs_{mm}, and Δs_{px} as measurement errors. It has been pointed out [1] that we must falsely assume a gaussian distribution of radii uncertainty in order to use propagation of error, however the deviation from Gaussian should be of order one over the radius and is inconsequential to our level of accuracy.

6 Conclusion

In conclusion it was shown that using a computer to increase accuracy in momentum measurement lead to a positive validation of conservation of energy. Furthermore, the slide projection table was calibrated to 1mm on the projection table is equivalent to 1.113 ± 0.0062mm in the bubble chamber. Without knowing the uncertainty in the pion beam energy, an uncertainty in this calibration is hard to define, though upwards of 30 trial averages reduces the standard error by a factor $\sqrt{30}$. It was found that the energy-distance relation suffers a great degree of uncertainty due to the accuracy and consistency the tracks widths are measured to, and also since the slides are not uniformly exposed, but it does help identify some particles.

Possible improvements to the computer program, named Bubbles to Momentum (BuM), would be to work on a better track centroid finder to make measurements swifter, more consistent, and less user dependant.

References

[1] D Bailey. Discussion on radii error. In University of Toronto undergraduate physics labs, March 2013.

[2] G. Jr. Clark and W. F. Diehl. Master Thesis: Range-energy relation for liquid hydrogen bubble chamber. Monterey, California: Naval Postgraduate School, 1957.

[3] M. Kuiack. Discussion of centroid of line fitting algorithm. University of Toronto Astronomy Undergraduate Laboratory, 2013.

[4] T.S. Yoon and J. Pitre. High Energy Physics Lab Manual. University of Toronto Advanced Physics Undergraduate Laboratory, 1992.

Identifier	$\|p\|$ (GeV/c)	$\Delta\|p\|$ (GeV/c)	p_x (GeV/c)	p_y (GeV/c)	Δp_x (GeV/c)	Δp_y (GeV/c)	Particle
View: 1 Film: 164 Slide: 872, Figure 2							
(1)	9.704	0.6358	9.703	-0.185	0.636	0.0272	π^+
(2)	1.163	0.0104	1.158	0.115	0.0105	0.00312	π^+
(3)	7.505	0.2308	7.501	-0.271	0.231	0.0124	p
(4)	0.256	0.0055	0.256	0.002	0.00551	0.0007	π^+
(4')	0.240	0.0093	0.231	0.067	0.0096	0.0041	–
(5)	0.468	0.0112	0.444	0.151	0.0117	0.0058	$\bar{p}$
(6)	0.115	0.0223	0.108	0.042	0.0233	0.015	μ^+
(7)	0.426	0.0107	0.390	-0.173	0.0113	0.0071	π^+
(8)	0.180	0.0032	0.180	0.0155	0.0032	0.0005	π^-
(Y)	0.716	0.0126	0.700	0.154	0.0129	0.0058	Λ^0 (+1S)
(Z)	0.592	0.0114	0.571	-0.158	0.0117	0.0072	K^0 (−1S)
(W)	0.114	0.0340	0.113	0.020	0.0343	0.0222	ν_μ
View: 2 Film: 254 Slide: 810, Figure 3							
(9)	10.330	0.1789	10.330	0.134	0.179	0.0045	π^+
(10)	0.265	0.0291	0.231	0.130	0.0305	0.0243	π^+
(10')	0.265	0.0284	0.212	0.159	0.0295	0.0265	–
(11)	3.791	0.6659	3.648	1.033	0.686	0.326	K^+ (−1S)
(12)	0.208	0.0075	0.152	0.142	0.0075	0.0074	μ^+
(13)	0.054	0.0011	0.0166	-0.052	0.0006	0.0012	π^-
(14)	0.771	0.0601	0.748	-0.189	0.0617	0.0248	p
(14')	0.772	0.0776	0.761	-0.132	0.0787	0.0249	–
(15)	0.894	0.0465	0.868	-0.215	0.0477	0.0184	π^+
(Q)*	0.134	0.0749	-0.106	0.083	0.0921	0.0309	π^-/π^0
(R)	0.062	0.0303	0.060	0.016	0.0305	0.0275	ν_μ
(T)	0.802	0.0593	0.765	-0.241	0.0617	0.0248	Λ^0 (+1S)
(S)	5.739	0.7069	5.685	-0.788	0.7123	0.3278	π^0

Table 1: Shown are the measurement of momentum of tracks from the two slides analyzed, and the inferred momentum of invisible particles. * Track (Q) may be mixture of two particles, likely π^- and π^0.

Identifier	μ (R. ion)	π (R. ion)	K (R. ion)	p (R. ion)	Width (mm) ($\pm$0.40mm)
View: 1 Film: 164 Slide: 872, Figure 2					
(1)	*	1.00	*	*	1.14
(2)	1.03	1.01	1.02	1.28	2.23
(3)	0.97	1.00	1.03	1.01	1.22
(4)	1.01	1.08	3.19	8.67	1.87
(5)	0.99	0.99	1.59	3.35	2.01
(6)	1.37	1.66	9.95	*	2.21
(7)	0.99	0.99	1.61	3.43	1.65
(8)	1.12	1.28	5.61	16.17	1.75
View: 2 Film: 254 Slide: 810, Figure 3					
(9)	*	1.00	*	*	1.14
(10)	1.01	1.07	3.04	8.17	1.92
(11)	0.97	1.00	1.03	1.01	1.99
(12)	1.05	1.15	4.36	12.31	1.34
(13)	3.28	5.03	*	*	1.80
(14)	1.02	1.00	1.14	1.79	1.19
(15)	1.02	1.00	1.11	1.69	1.11

Table 2: Shown are the relative ionizations for the tracks under the assumption of different particle types as interpolated onto figure 1. A value of 1 is minimum ionizing implying the track line should be very thin, with large spacing between bubbles. The incoming pions are defined as the reference point for minimum ionizing tracks. There is an * for values off-the-scale in figure 1, and for known particle types (the incoming pions). The widths of the tracks are an attempt to correlate relative ionization with track thickness, the uncertainty is an estimate based on the human eye's ability to correctly choose the boundary of the track.